


Diversification of division mechanisms in endospore-forming bacteria revealed by analyses of peptidoglycan synthesis in *Clostridioides difficile*

Received: 21 August 2023

Shailab Shrestha^{1,2}, Najwa Taib^{3,4}, Simonetta Gribaldo³ & Aimee Shen¹✉

Accepted: 14 November 2023

Published online: 02 December 2023

 Check for updates

The bacterial enzymes FtsW and FtsI, encoded in the highly conserved *dcw* gene cluster, are considered to be universally essential for the synthesis of septal peptidoglycan (PG) during cell division. Here, we show that the pathogen *Clostridioides difficile* lacks a canonical FtsW/FtsI pair, and its *dcw*-encoded PG synthases have undergone a specialization to fulfill sporulation-specific roles, including synthesizing septal PG during the sporulation-specific mode of cell division. Although these enzymes are directly regulated by canonical divisome components during this process, *dcw*-encoded PG synthases and their divisome regulators are dispensable for cell division during normal growth. Instead, *C. difficile* uses a bifunctional class A penicillin-binding protein as the core divisome PG synthase, revealing a previously unreported role for this class of enzymes. Our findings support that the emergence of endospore formation in the *Firmicutes* phylum facilitated the functional repurposing of cell division factors. Moreover, they indicate that *C. difficile*, and likely other clostridia, assemble a distinct divisome that therefore may represent a unique target for therapeutic interventions.

Synthesis of cell wall peptidoglycan (PG) is essential for growth and division in most bacteria. The extra-cytoplasmic assembly of PG results from two sequential enzymatic reactions: a transglycosylation reaction that polymerizes the PG precursor Lipid II into glycan strands and a transpeptidation reaction that crosslinks these glycan strands together to form a protective meshwork¹.

Our understanding of this critical process has been transformed by the recent discovery that shape, elongation, division, and sporulation (SEDS) family proteins function as PG glycosyltransferases in complex with cognate class B penicillin-binding protein (bBPB) transpeptidases to synthesize PG^{2–5}. Current models posit that specific SEDS-bBPB pairs function as the core PG synthases driving either cell elongation or division in rod-shaped bacteria^{2,4–8}. These specialized

pairs of SEDS-bBPBs associate with specific multiprotein assemblies to mediate either cell elongation or cell division: lateral growth is typically driven by the SEDS-bBPB pair, RodA-MrdA, as a part of the elongasome, while septum formation is mediated by the SEDS-bBPB pair, FtsW-FtsI, as a part of the divisome.

Prior to the discovery of SEDS glycosyltransferases, class A penicillin-binding proteins (aPBPs) were the only known PG synthases with glycosyltransferase activity. Unlike monofunctional bBPB transpeptidases, aPBPs are bifunctional enzymes that harbor both glycosyltransferase and transpeptidase activities and they were presumed to be the primary PG synthases driving cell elongation and division⁹. However, recent evidence suggests that aPBPs often play non-essential, peripheral roles during these processes which is consistent with

¹Department of Molecular Biology and Microbiology, Tufts University School of Medicine, Boston, MA, USA. ²Program in Molecular Microbiology, Tufts University Graduate School of Biomedical Sciences, Boston, MA, USA. ³Institut Pasteur, Université Paris Cité, Evolutionary Biology of the Microbial Cell Unit, Paris, France. ⁴Institut Pasteur, Université Paris Cité, Bioinformatics and Biostatistics Hub, F-75015 Paris, France. ✉e-mail: aimee.shen@tufts.edu

their absence from the genomes of many obligate intracellular bacteria^{3,10–12}. Indeed, aPBPs can function independently of the divisome and elongasome and appear to mainly modify and repair PG synthesized by SEDS-bBPB enzymes^{9,12,13}.

Notably, these models of bacterial PG synthesis primarily derive from studies in *Escherichia coli* and *Bacillus subtilis*, but studies in organisms with different cell morphologies and mechanisms of growth have variably supported and challenged these general models. For instance, all Actinobacteria and some Proteobacteria follow a polar growth model where cell growth is driven by PG synthesis at cell poles. In these organisms, cell elongation is largely mediated by aBPB activity^{14–17}. Given the diversity of mechanisms involved in bacterial PG synthesis and the importance of studying these processes in diverse bacteria, the functional characterization of major PG synthases in different bacteria is an area of significant interest.

Although diverse mechanisms of cell elongation have been described in bacteria, cell division mechanisms appear to be broadly conserved. Divisome-guided septal PG synthesis is mediated by the essential SEDS-bBPB enzyme pair, FtsW-FtsI, which is considered to be universally conserved in all bacteria⁵. Genes encoding these enzymes are typically located within the division and cell wall (*dcw*) cluster¹⁸, which contains numerous genes involved in PG synthesis and cell division. Recent phylogenetic analyses have revealed that the *dcw* locus is widely conserved across almost all bacterial phyla and likely originated in the Last Common Bacterial Ancestor billions of years ago¹⁸.

Despite this extreme conservation, the SEDS gene in the *dcw* cluster of the model endospore-forming bacterium *Bacillus subtilis* does not encode FtsW, but rather SpoVE, a sporulation-specific SEDS glycosyltransferase that is critical for endospore formation^{19–21}. In *B. subtilis*, SpoVE forms a complex with the sporulation-specific bBPB SpoVD to synthesize a thick protective PG layer known as the cortex during sporulation^{22–24}. Notably, *B. subtilis* is a member of the Firmicutes phylum, which is the only bacterial phyla to have evolved endospore formation. Since the formation of highly resistant, mature spores depends on a series of PG transformations unique to endospore-forming bacteria, we hypothesized that the Firmicutes would exhibit greater variation in the composition and function of bBPB and SEDS genes in their *dcw* loci. In this work, we analyzed the distribution of PG synthase-encoding genes in the *dcw* loci of Firmicutes organisms and analyzed their function in the medically important clostridial pathogen, *Clostridioides difficile*. Here, we reveal a previously unappreciated diversification in the mechanisms by which *C. difficile*, and likely other clostridia, mediates cell division during vegetative growth and endospore formation.

Results

Diversity of *dcw*-encoded PG synthases based on sporulation potential

Firmicutes are unique among bacteria in forming endospores. While the last common ancestor of the Firmicutes is thought to have been an endospore former, the ability to sporulate has been independently lost among members of this phylum²⁵ (Fig. 1, Supplementary Fig. 1, Supplementary Data 2, 3). To analyze the distribution of genes encoding SEDS glycosyltransferases and bBPBs in the *dcw* cluster of both spore-forming and non-spore-forming Firmicutes organisms, we constructed a custom database consisting of 494 Firmicutes genomes representative of the six major classes described in this phylum. Next, we inferred the organism's ability to form endospores by determining the presence of *spoOA* and *spolIE* in all Firmicutes genomes. These genes are both part of a core genomic signature of sporulating bacteria²⁶ and encode key regulators required for initiating and committing cells to sporulation, respectively^{27,28}, so their co-occurrence strongly suggests that a given species is a spore former. We searched for SEDS and bBPB homologs in all Firmicutes genomes and identified genes encoding

SEDS and bBPB enzymes in the *dcw* cluster based on their synteny with other genes of the *dcw* cluster (*mraW*, *mraY*, *ftsZ*, *mraZ*, and *murCDEF*). We also identified a pair of SEDS and bBPB homologs, RodA and MrdA, respectively, involved in cell elongation and located in a different locus. Finally, we identified SEDS homologs encoded adjacent to the gene encoding pyruvate carboxylase, PycA (Fig. 1, Supplementary Figs. 1, 2, Supplementary Data 2).

In agreement with what has been described in *Bacillus subtilis*²², sporulating taxa from Bacilli encode two homologs of bBPBs in the *dcw* cluster, which most probably correspond to the canonical cell division PG synthesizing enzyme, FtsI, and the sporulation-specific PG synthesizing enzymes, SpoVD (Fig. 1). Non-sporulating Bacilli only have a single bBPB gene in their *dcw* clusters, suggesting that *spoVD* was lost from this locus coincident with the loss of sporulation; the remaining bBPB gene in the *dcw* locus presumably encodes *ftsI*. In contrast, sporulating Bacilli encode only a single SEDS glycosyltransferase gene in their *dcw* loci. This gene likely encodes SpoVE based on functional analyses in *B. subtilis*^{19–21} and our finding that non-sporulating Bacilli lack SEDS genes altogether from their *dcw* loci (Fig. 1). Thus, SEDS genes appear to have been lost from the *dcw* cluster coincident with the loss of sporulation. Notably, all Bacilli carry a SEDS glycosyltransferase gene outside of the *dcw* cluster (usually adjacent to *pycA* (Fig. 1)) that codes for a canonical cell division FtsW ortholog; the essential function of this conserved gene has been validated in several members of the Bacilli^{5,8,29,30}, suggesting that *dcw*-encoded PG synthesizing enzymes became specialized to function exclusively during spore formation.

The same arrangement between sporulating and non-sporulating species can be observed among members of the Negativicutes and Linochordia (Fig. 1), suggesting that the *dcw*-encoded SEDS and bBPB homologs present in the sporulating members of these Classes also encode SpoVE and SpoVD. Together, these analyses reveal that the presence of SEDS and bBPB genes in the *dcw* cluster is highly correlated with sporulation (Supplementary Data 3), and that the genes present in the *dcw* cluster of sporulating Firmicutes likely code for SpoVE and SpoVD, respectively, rather than the canonical cell division proteins FtsW and FtsI. Exceptions are represented by some members of the Clostridia, Tissierellia, and Erysipelotrichia, which display a mixed pattern (Supplementary Fig. 1, Supplementary Data 2). Surprisingly, many members of the Clostridia do not appear to have any extra copy of genes encoding division-specific SEDS and bBPB enzymes in their *dcw* clusters or elsewhere in the genomes, suggesting they completely lack the canonical cell division pair FtsW-FtsI. Therefore, we sought to define the functions of *dcw*-encoded SEDS and bBPB genes of the genetically tractable clostridial species *C. difficile*.

dcw-encoded PG synthases control *C. difficile* septal PG synthesis during sporulation but not vegetative growth

To this end, we determined the effect of deleting the *dcw*-encoded SEDS and bBPB genes, *spoVE* and *spoVD*, on *C. difficile* growth and sporulation. Consistent with the results of a prior transposon screen indicating that *spoVE* and *spoVD* are non-essential for growth³¹, we were able to create single deletion strains lacking *spoVD* or *spoVE*. These strains did not exhibit growth or morphological defects during vegetative growth (Fig. 2a, b), indicating that *C. difficile* SpoVD and SpoVE are not involved in vegetative cell division. Consistent with prior work^{32,33}, the *C. difficile* Δ *spoVD* strain failed to make heat-resistant spores (Supplementary Fig. 3) or synthesize a cortex layer based on transmission electron microscopy (TEM) analyses (Supplementary Fig. 4). Similar phenotypes were observed for the Δ *spoVE* strain, indicating that *C. difficile* SpoVD and SpoVE share similar functions with their orthologs in *B. subtilis* in mediating cortex synthesis^{21–24}. Importantly, the sporulation defect of these mutants could be fully complemented from a chromosomal ectopic locus (Supplementary Fig. 3).

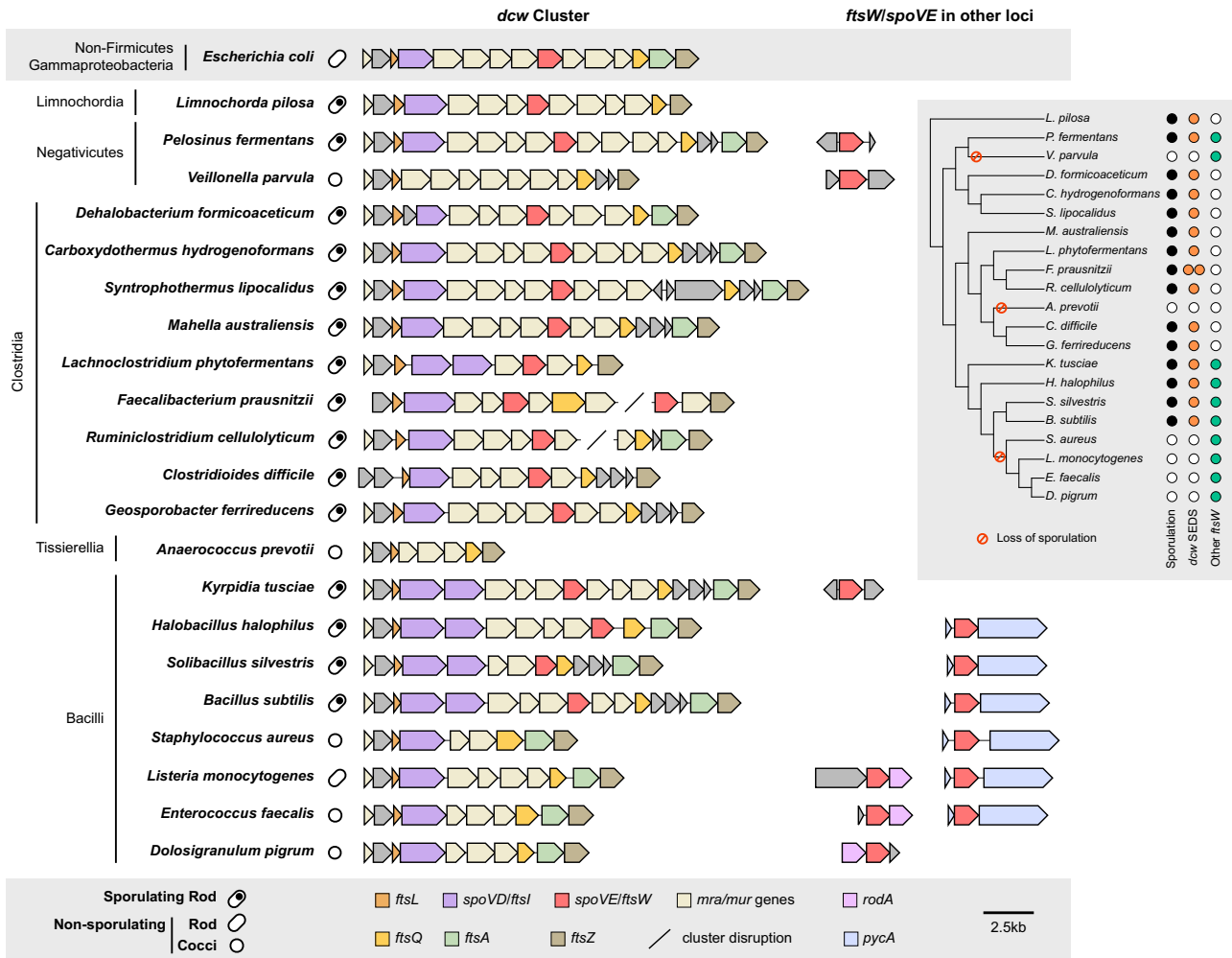


Fig. 1 | Comparison of *dcw* cluster composition and occurrence of SEDS family proteins across diverse Firmicutes species. Cell shape (rod or cocci) and sporulation ability are indicated. The ability to form spores was inferred by the presence of broadly conserved sporulation-specific genes *spoOA* and *spolIE* in the genome²⁶. All SEDS homologs that cluster with divisome-associated FtsW encoding genes are

shown for each organism (Supplementary Fig. 2). For genome accession numbers, coordinates, and taxonomy information, see Supplementary Data 1. The inset tree shows phylogenetic relationships and the colored circles highlight the presence of sporulation genes (black), and *ftsW/spoVE* within (orange) and outside (green) the *dcw* cluster. For analyses of the full dataset, see Supplementary Fig. 1.

However, in contrast with *B. subtilis*, we observed that *C. difficile* $\Delta spoVD$ and $\Delta spoVE$ mutants appeared to sporulate at lower levels than wild-type (WT), with few cells exhibiting visible signs of sporulation during phase-contrast microscopy analyses (Supplementary Fig. S3). To investigate whether SpoVD and SpoVE affect sporulation processes earlier than cortex synthesis, we evaluated the ability of $\Delta spoVD$ and $\Delta spoVE$ cells to progress through the different morphological stages of sporulation via cytological profiling of sporulating cells^{34,35}. These analyses revealed that most $\Delta spoVD$ and $\Delta spoVE$ cells showing morphological signs of sporulation were stalled at the asymmetric division stage, with a relatively small proportion completing engulfment compared to WT cells (Fig. 2c, Supplementary Fig. 5). Strikingly, the overall proportions of $\Delta spoVD$ and $\Delta spoVE$ cells exhibiting morphological signs of sporulation, i.e., cells that have completed or progressed beyond asymmetric division, were ~3-fold lower than WT (Fig. 2d). This effect at an earlier stage of sporulation is consistent with transcriptional analyses indicating that *C. difficile* *spoVD* and *spoVE* are expressed immediately at the onset of sporulation^{36,37}, in contrast with *B. subtilis* *spoVD* and *spoVE*, which are expressed in the mother-cell compartment after sporulating cells complete asymmetric division.

The decrease in apparent sporulation frequency in $\Delta spoVD$ and $\Delta spoVE$ mutants could be due to the enzymes regulating (1) asymmetric

division through the synthesis of septal PG and/or (2) sporulation initiation via an unknown mechanism. To rule out the latter possibility, we compared the frequency of sporulation initiation in $\Delta spoVD$ and $\Delta spoVE$ cells relative to WT cells. Using a SpoOA-dependent *P_{spoIIIE}::mScarlet* transcriptional reporter, we found that $\Delta spoVD$ and $\Delta spoVE$ strains activate SpoOA, the master transcriptional regulator that initiates sporulation²⁷, at similar frequencies and levels relative to WT (Fig. 2e, f). In contrast, significantly fewer $\Delta spoVD$ and $\Delta spoVE$ cells compared to WT induced the expression of a reporter that is activated after the formation of the polar septum (*P_{sipL}::mScarlet*) (Supplementary Fig. 6a)^{36,37}. Consistent with the reporter data, RT-qPCR and western blot analyses of the $\Delta spoVD$ and $\Delta spoVE$ mutants confirmed that they activate SpoOA at WT levels but exhibit defects in activating later-acting sporulation-specific sigma factors that only become activated upon completion of asymmetric division (Supplementary Fig. 7, 8). Overall, our data suggest that *C. difficile* SpoVD and SpoVE play important roles in synthesizing septal PG during asymmetric division, in addition to their canonical function in synthesizing the spore cortex. Consistent with this model, we detected incomplete polar septum formation in $\Delta spoVD$ and $\Delta spoVE$, but not WT, cells in transmission electron microscopy analyses (Fig. 2g). Moreover, in agreement with a previous study³³, *C. difficile* SpoVD localizes to polar septa during asymmetric division (Supplementary Fig. 9).

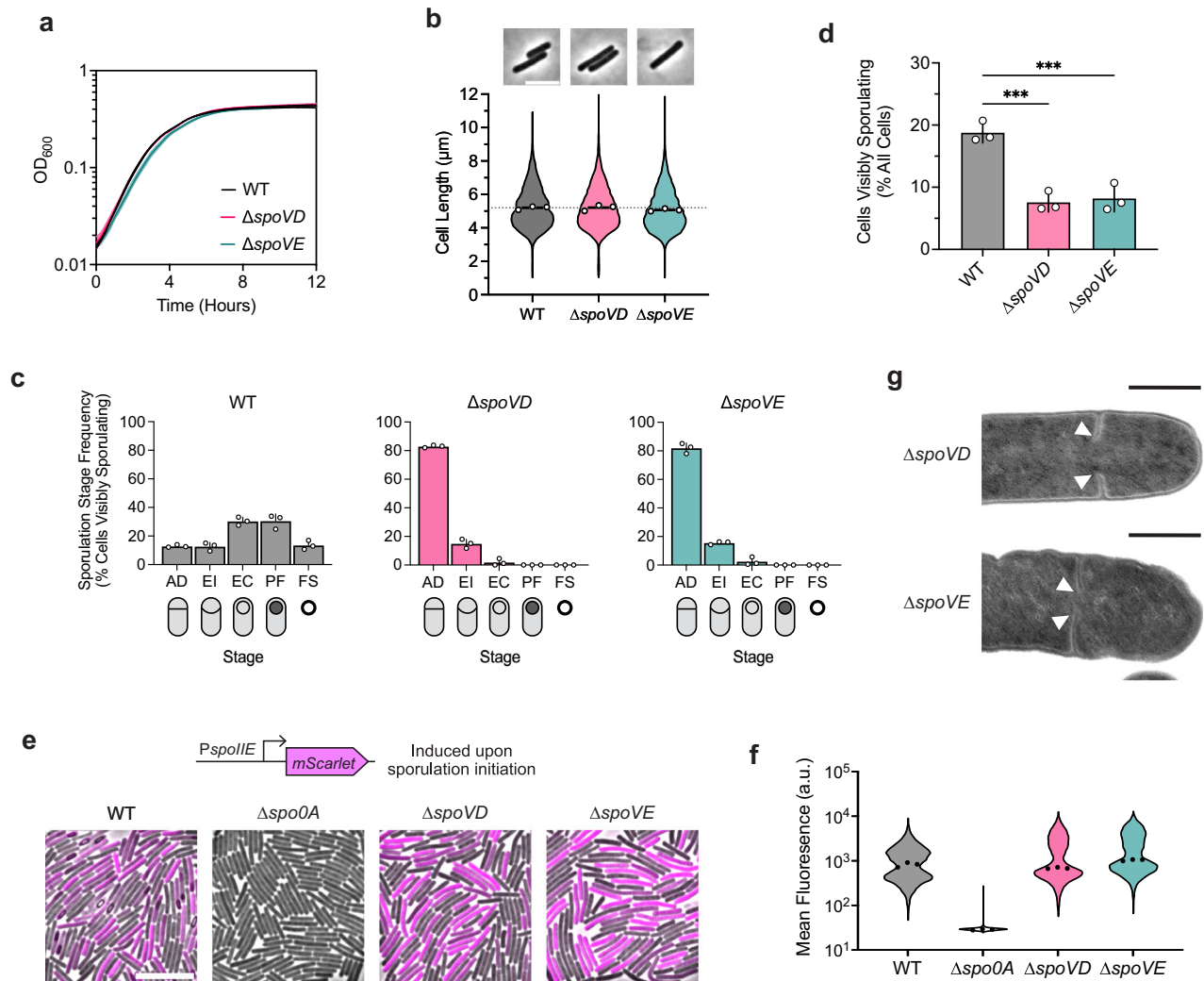


Fig. 2 | The sporulation-specific PG synthases, SpoVD and SpoVE, are important for asymmetric, but not vegetative, division. **a** Growth profiles of *C. difficile* wildtype (WT), $\Delta spoVD$, and $\Delta spoVE$ strains in BHIS. Data are from a single experiment; mean and standard deviation curves are plotted from three biological replicates. **b** Violin plots showing length distributions and representative micrographs of cells sampled from BHIS cultures during mid-exponential growth (OD₆₀₀ ~0.5). White circles indicate means from each replicate; black lines indicate average means; dotted line indicates the WT average mean for comparison across strains. Data from three biological replicates; >1500 cells per sample. Scale bar, 5 μm . **c, d** Cytological profiling of cells sampled from sporulation-inducing plates after 18–20 h of growth. Cells were assigned to five distinct stages based on their membrane (FM4-64) and DNA (Hoechst) staining and phase-contrast morphological phenotypes. For representative micrographs and stage assignment information, see Supplementary Fig. 5a. AD Asymmetric Division, EI Engulfment Initiated, EC Engulfment Completed, PF Phase bright/dark Forespore, FS Free Spore. White circles indicate means from each replicate, bars indicate average means and error

bars indicate standard deviation. *** $p < 0.001$; statistical significance was determined using ordinary one-way ANOVA with Dunnett's test. Data from three independent experiments; >1000 total cells and >100 visibly sporulating cells per sample. Source data with exact P values are provided in the Source Data file. **e** Representative merged phase-contrast and fluorescence micrographs visualizing $P_{spoIIIE}::mScarlet$ transcriptional reporters in sporulating cells sampled from 70:30 plates after 14–16 h of growth. $P_{spoIIIE}$ is induced upon sporulation initiation. The $\Delta spoOA$ strain serves as a negative control because it does not initiate sporulation. Scale bar, 10 μm . **f** Violin plots showing quantified mean fluorescence intensities of strains shown in **e**. Black dots represent median values from each replicate. Data from three independent experiments; >3000 cells per sample. **g** Transmission electron micrographs of $\Delta spoVD$ and $\Delta spoVE$ sporulating cells that fail to complete septum formation 24 h after sporulation induction (white arrows). Scale bars, 500 nm. >50 sporulating cells were analyzed per strain from two independent experiments for WT and $\Delta spoVD$ and one experiment for $\Delta spoVE$.

Conserved divisome components regulate cell division during spore formation but not vegetative growth in *C. difficile*

Septal PG synthesis requires the coordinated assembly and localization of numerous divisome components at the division site. If SpoVD and SpoVE mediate septal PG synthesis during asymmetric division, we reasoned that their activities are likely regulated by components of the divisome. Previous studies have implicated the widely conserved divisome sub-complex composed of FtsL, FtsQ, and FtsB (also known as FtsL, DivB, and DivC in some Firmicutes) in directly regulating the activity and localization of FtsW-FtsZ^{38–42}. Intriguingly, although *C. difficile* appears to lack functional FtsW and FtsI orthologs, it encodes

orthologs of their regulators (Supplementary Fig. 10). *cd630_26570* and *cd630_26500* are both located in conserved locations within the *dcw* cluster (Fig. 1) and encode putative membrane proteins with homology to FtsL and FtsQ, respectively. We also identified *cd630_34920* as encoding an FtsB homolog. We refer to these genes as *ftsL* (*cd630_26570*), *ftsQ* (*cd630_26500*), and *ftsB* (*cd630_34920*) from hereon (Supplementary Fig. 10).

Although *ftsL*, *ftsQ*, and *ftsB* encode proteins that are typically considered essential components of the divisome, a previous transposon screen in *C. difficile* identified these genes as non-essential but important for spore formation³¹. Consistent with this finding, we

readily obtained $\Delta ftsL$, $\Delta ftsQ$, and $\Delta ftsB$ deletion strains. These mutants showed no significant growth or morphological defects (Fig. 3a, b), indicating that FtsL, FtsQ, and FtsB likely fulfill non-canonical, sporulation-specific roles in *C. difficile*. Indeed, all three mutants formed heat-resistant spores less efficiently than WT, with $\Delta ftsL$ and $\Delta ftsB$ showing ~100-fold defects and $\Delta ftsQ$ showing a modest ~2-fold decrease (Supplementary Fig. 3). These sporulation defects could be complemented by expressing wildtype copies of their respective genes from a chromosomal ectopic locus (Supplementary Fig. 3). The milder phenotypes observed for $\Delta ftsQ$ are consistent with prior observations that FtsQ is only conditionally essential or completely absent in some bacterial species^{43–45}. Notably, phase-contrast microscopy of sporulating cells revealed that all three mutants form phase-bright spores, albeit infrequently, and TEM analysis confirmed that the mutants can synthesize cortex PG, unlike $\Delta spoVD$ and $\Delta spoVE$ cells (Supplementary Fig. 4a). However, similar to $\Delta spoVD$ and $\Delta spoVE$ strains, incomplete polar septa were detected in TEM analyses of $\Delta ftsL$, $\Delta ftsQ$, and $\Delta ftsB$ strains, suggesting that these proteins are important for completing asymmetric division (Supplementary Fig. 4b).

Consistent with this observation, cytological profiling revealed that sporulating $\Delta ftsL$, $\Delta ftsQ$, and $\Delta ftsB$ cells complete and progress beyond asymmetric division at a significantly lower frequency compared to WT (Fig. 3c, d, Supplementary Fig. 5). A small proportion (~2%) of $\Delta ftsL$ and $\Delta ftsB$ cells were able to progress beyond engulfment to make mature spores (Fig. 3d). The phenotype for $\Delta ftsQ$ was slightly less severe than for $\Delta ftsL$ and $\Delta ftsB$, with ~4% of $\Delta ftsQ$ cells making phase-bright (cortex-positive) spores (Fig. 3d). However, a higher proportion of $\Delta ftsQ$ sporulating cells remained stalled at asymmetric division, suggesting that *C. difficile* FtsQ shares similar functions with its *B. subtilis* ortholog, DivIB, in regulating PG transformations during engulfment⁴⁶. Since the PG synthesizing activity of FtsW-FtsI depends on direct interactions between the enzymes and the ternary FtsLQB sub-complex in the bacteria studied to date, we tested whether SpoVD and SpoVE form a divisome-like complex with FtsL, FtsQ, and FtsB by probing pairwise interactions using bacterial two-hybrid assays. This assay confirmed that SpoVD and SpoVE interact, consistent with these enzymes forming a cognate SEDS-bBPB pair as previously shown in *B. subtilis*²⁴ (Fig. 3e, f) and that *C. difficile* FtsL, FtsQ, and FtsB likely form a ternary sub-complex similar to homologs in other bacteria^{47–50}. Importantly, we observed that *C. difficile* SpoVD interacts with FtsL and FtsQ, suggesting that the ternary sub-complex likely directly regulates the activity of SpoVE-SpoVD. Taken together, these data strongly suggest that *C. difficile* assembles a distinct polar divisome that partially relies on the sporulation-specific SEDS-bBPB pair, SpoVE-SpoVD, to synthesize the polar septum during endospore formation.

***C. difficile*'s sole essential SEDS-bBPB pair mediates elongation**

Although septal PG synthesis by SpoVD and SpoVE is important for asymmetric division, *C. difficile* cells that lack these proteins are still able to synthesize polar septa, albeit at lower rates. It is likely that the PG synthases that mediate vegetative cell division also contribute to septal PG synthesis during asymmetric division. Since *C. difficile* appears to lack obvious orthologs of the widely conserved divisome-specific SEDS-bBPB pair, we considered the involvement of all major PG synthases encoded in the *C. difficile* genome. *C. difficile* has a relatively minimal set of PG synthases: a single class A PBP (PBPI), three class B PBPs (PBP2, PBP3, and SpoVD), two SEDS proteins (RodA and SpoVE), and one monofunctional glycosyltransferase (MGT) (Fig. 4a). Among these synthases, we considered PBPI, PBP2, and RodA to be the most likely candidates for enzymes that contribute to septal PG synthesis during medial division since genes encoding these proteins were previously identified as being essential for vegetative growth³¹. Consistent with this and the prior finding that loss of PBP3 results in a sporulation defect³², we confirmed that single deletions of genes encoding PBP3 and MGT do not significantly alter the growth of

vegetative cells, although they induce a modest increase in cell length (Supplementary Fig. 11).

Although RodA and PBP2 are the sole essential SEDS-bBPB pair, the genomic location of their respective genes adjacent to the *mreBCD* operon, which encodes critical components of the elongasome, predicts that they mediate elongation based on analyses in other bacteria². Furthermore, *C. difficile* RodA branches with SEDS enzymes implicated in mediating cell elongation in other organisms and in a separate group from *dcw*-encoded SEDS proteins (Supplementary Fig. 2a, b), consistent with recent work suggesting that the functional divergence of SEDS paralogs to roles in cell division or elongation predates the Last Bacterial Common Ancestor¹⁸. To experimentally confirm the roles of RodA and PBP2 in cell elongation, we used CRISPR interference (CRISPRi)⁵¹ to knock down the expression of their respective genes. Consistent with their essentiality, individual knockdowns produced significant growth defects upon induction of the CRISPR system (Fig. 4b). CRISPRi knockdown of either *rodA* or *pbp2* resulted in lateral bulging, rounding, and frequent lysis of cells (Fig. 4c). These phenotypes are characteristic of cells defective in cell elongation as observed in other rod-shaped bacteria^{30,52–55} and stand in contrast to the phenotypes of divisome component CRISPRi knock-downs, which induce filamentation due to defects in septum formation. Thus, RodA and PBP2 are the core PG synthases during cell elongation in *C. difficile*.

***C. difficile*'s aBPB drives septal PG synthesis during vegetative division**

These analyses left the aBPB, PBPI, as the primary candidate for synthesizing septal PG during vegetative division in *C. difficile*. Since aPBPs are capable of both polymerizing and cross-linking PG, PBPI should be able to substitute for both enzymatic activities fulfilled by a divisome-associated SEDS-bBPB pair. Indeed, PBPI was previously suggested to be essential for vegetative growth³¹, and its depletion results in cell filamentation⁵¹. Knockdown of the gene encoding PBPI validated these prior reports, as it resulted in severe growth defects and cell filamentation phenotypes characteristic of cells deficient in cell division (Fig. 5a, b). Moreover, subcellular localization of PBPI during vegetative growth showed significant enrichment at division septa (Fig. 5e, f).

Chemical inhibition of PBPI activity with the glycosyltransferase inhibitor moenomycin also produced filamentous cells, suggesting a crucial role of PBPI glycosyltransferase activity in cell division (Fig. 5d). These data contradict a prior report⁵⁶, which suggested that *C. difficile* cells are intrinsically resistant to moenomycin. Although moenomycin also inhibits the catalytic activity of MGTs, sensitivity to moenomycin was unchanged in an MGT-null mutant, suggesting that the drastic phenotypes observed in moenomycin-treated cells are exclusively due to the inhibition of PBPI activity (Supplementary Fig. 12a). Consistent with this, growth defects from moenomycin treatment were rescued by overproduction of PBPI (Supplementary Fig. 12c). Furthermore, these analyses revealed that *C. difficile* is sensitive to PBPI overproduction likely due to dysregulation of PBPI activity.

Next, we considered whether components of the polar divisome described above contribute to vegetative cell division. We reasoned that if this was the case, mutants lacking these components should be hypersensitive to moenomycin treatment. We found that the susceptibility of $\Delta spoVD$, $\Delta spoVE$, $\Delta ftsL$, $\Delta divIB$, and $\Delta divIC$ cells to moenomycin is unchanged compared to WT (Supplementary Fig. 12a, b). Overall, these results are consistent with a non-canonical divisome composition in *C. difficile*, where PBPI is the major septal PG synthase during vegetative cell division.

Discussion

The *dcw* cluster is well-conserved across all known bacterial phyla and was likely encoded in the Last Bacterial Common Ancestor¹⁸. While the

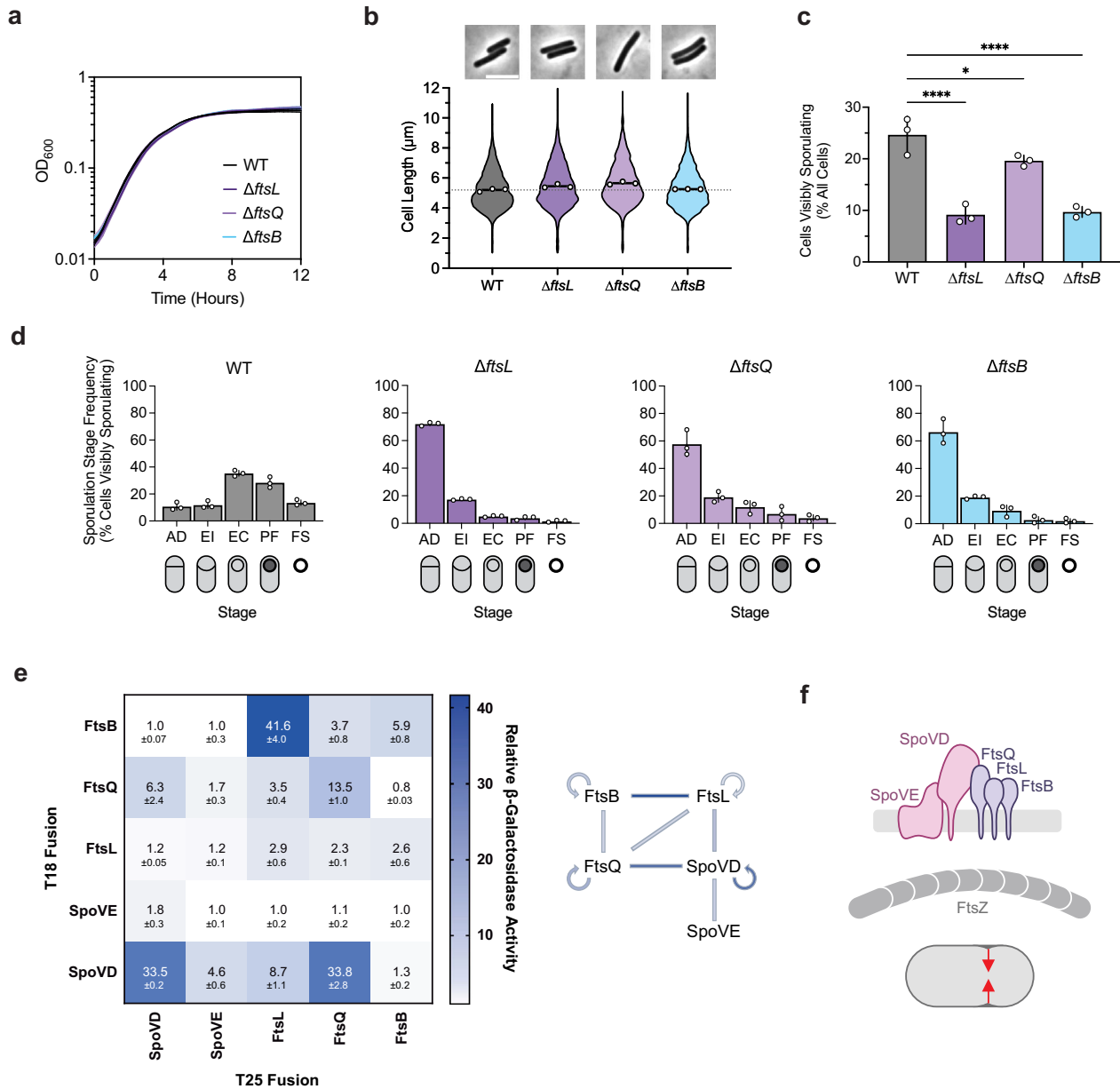


Fig. 3 | The canonical divisome components, FtsL, FtsQ, and FtsB, are dispensable for vegetative cell division but are important for asymmetric division. a Growth profiles of the indicated strains in BHIS. Data are from a single growth curve experiment; mean, and standard deviation curves are plotted from three biological replicates. **b** Violin plots showing cell length distributions and representative micrographs of cells sampled from BHIS cultures during exponential growth ($OD_{600} \sim 0.5$). White circles indicate means from each replicate, black lines indicate average means, and the dotted line indicates the WT average mean for comparison across strains. Data from three biological replicates; >1500 cells per sample. Scale bar, 5 μm . **c, d** Cytological profiling of sporulating cells sampled from sporulation-inducing 70:30 plates after 18–20 h of growth. Cells were assigned to five distinct stages based on their membrane (FM4-64) and DNA (Hoechst) staining and their phase-contrast morphological phenotypes. For representative micrographs and stage assignment information, see Supplementary Fig. 5b. AD Asymmetric Division, EI Engulfment Initiated, EC Engulfment Completed, PF Phase-

bright/dark Forespore, FS Free Spore. White circles indicate means from each replicate, bars indicate average means and error bars indicate standard deviation. * $p < 0.05$, *** $p < 0.0001$; statistical significance was determined using an ordinary one-way ANOVA with Dunnett’s test. Data from three independent experiments; >1000 total cells and >100 visibly sporulating cells per sample. Source data with exact P values are provided in the Source Data file. **e** Bacterial two-hybrid analysis of interactions between components of the predicted polar divisome. The β -galactosidase activity was normalized to the negative control. Mean \pm standard deviation from three biological replicates is indicated. The schematic shows interactions between different proteins where lines are colored according to the amount of β -galactosidase activity detected. **f** Schematic showing FtsL, FtsQ, and FtsB forming a divisome-like subcomplex with SpoVD and SpoVE. This polar divisome contributes to septal PG synthesis during asymmetric division. Created with BioRender.com.

order and composition of core *dcw* genes involved in PG synthesis and cell division have remained largely unchanged through billions of years of vertical inheritance, our analyses suggest that two key constituents of the cluster, *ftsW* and *ftsI*, have undergone a surprising functional divergence during the evolution of endospore formation. Rather than encoding the core PG synthases required for cell division

as they do in most bacteria, the SEDS and bBPB genes in the *dcw* cluster of sporulating Firmicutes likely encode enzymes specialized to function exclusively during endospore formation. This conclusion is supported by our finding that Firmicutes predicted to have lost the ability to sporulate also lack SEDS genes from their *dcw* cluster (Fig. 1, Supplementary Fig. 1, Supplementary Data 3). Furthermore, we show that,

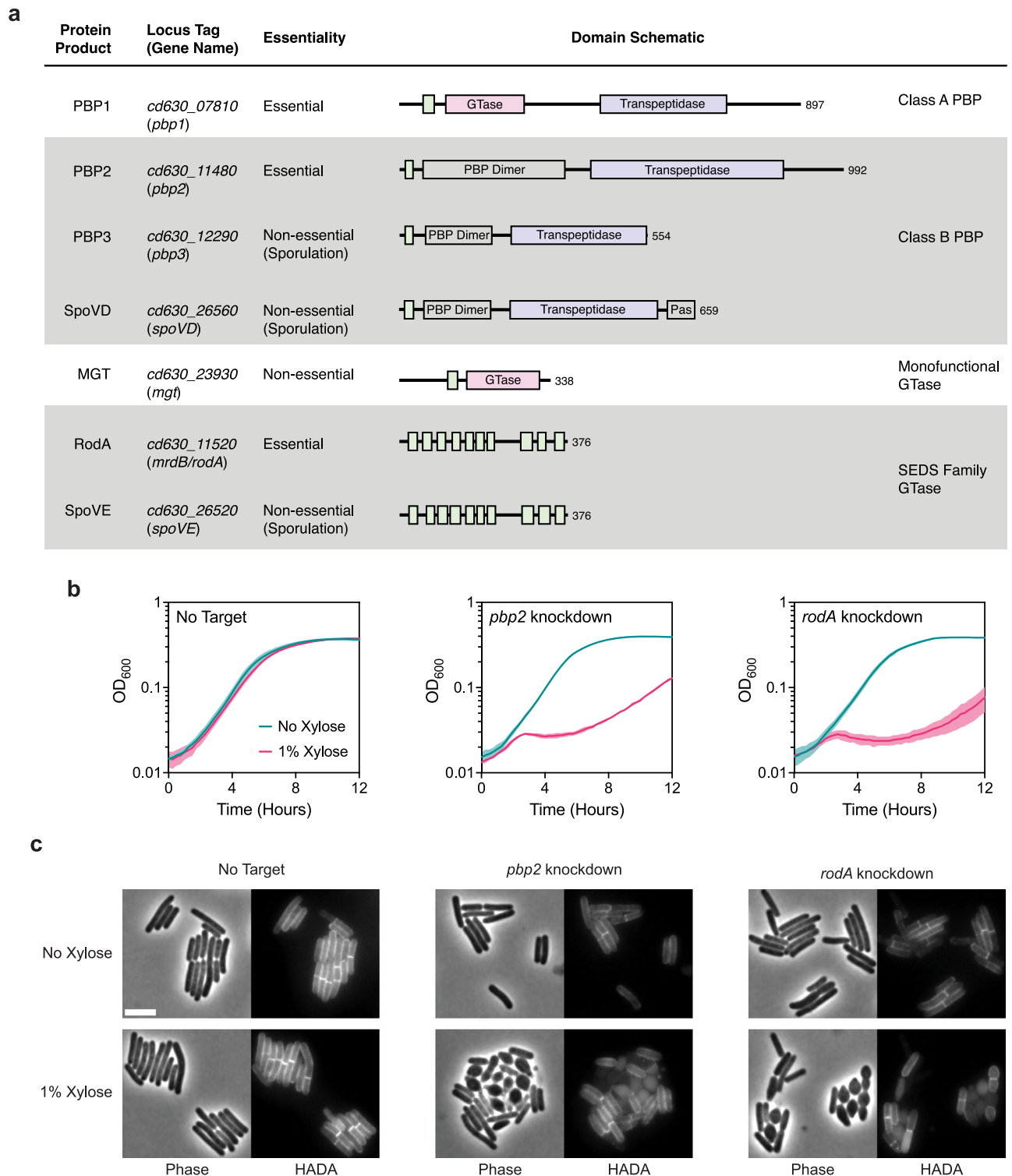


Fig. 4 | RodA and PBP2 are involved in cell elongation. **a** Major PG synthases encoded in the *C. difficile* strain 630 genome. Protein domains and catalytic sites predicted using HMMER are indicated in the schematic for each protein (hmmer.org). GTase, Glycosyltransferase Domain (Pink); PBP Dimer, PBP Dimerization Domain; Pas, PASTA Domain; Transpeptidase domain (Purple). Predicted transmembrane regions are depicted as green boxes. **b** Growth profiles of *pbp2* and *rodA* CRISPRi knockdown strains compared to a no target control strain. Data are from a single growth curve

experiment; mean and standard deviation plotted from three biological replicates. **c** Representative micrographs showing morphological and PG incorporation phenotypes of control, *pbp2*, and *rodA* knockdown cells. Cells were grown in BHIS with or without xylose for 6–8 h. PG was labeled by incubation with a fluorescent D-amino acid (HADA). Scale bar, 5 μ m. Data representative of multiple independent experiments.

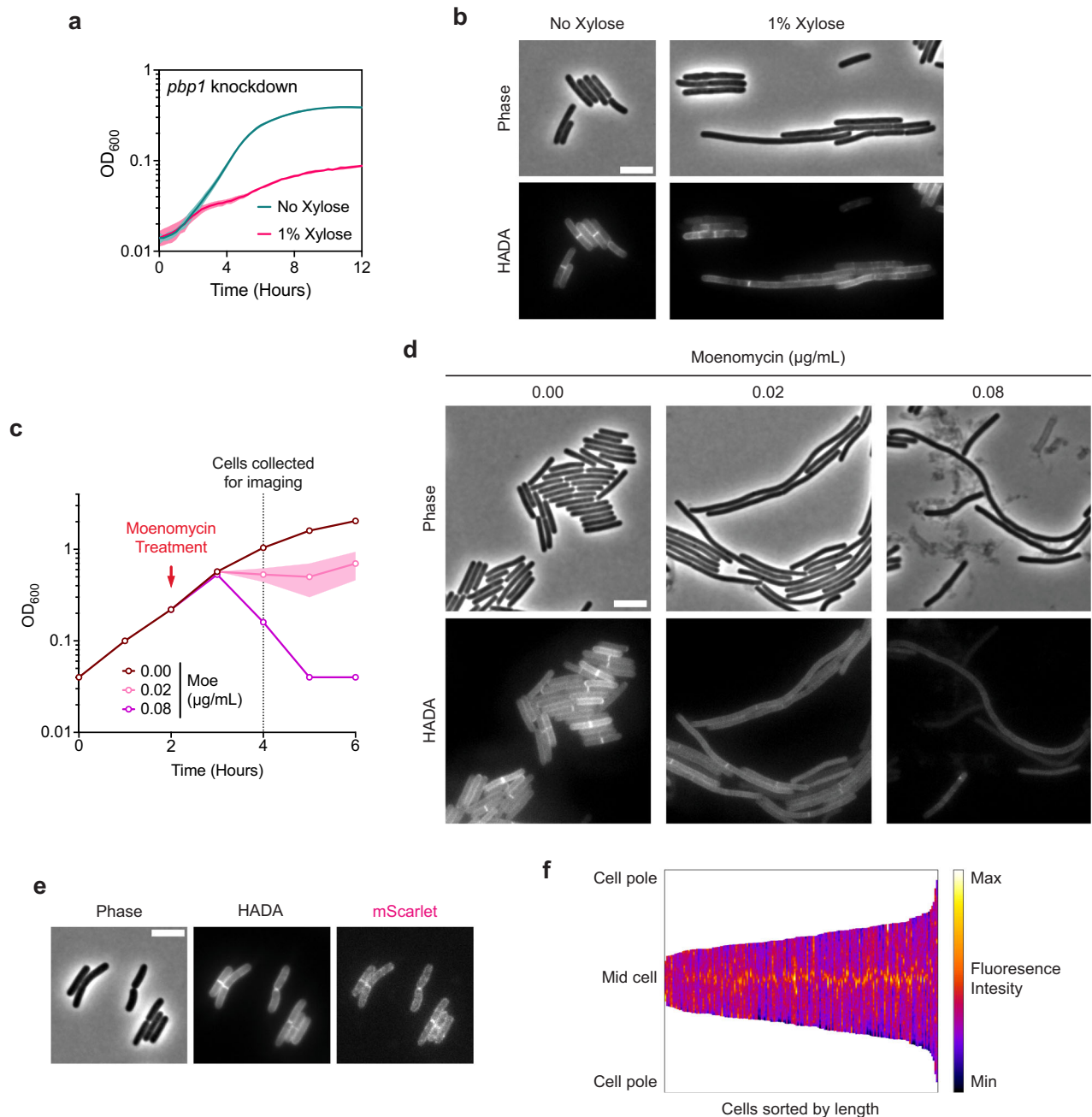


Fig. 5 | The class A PBP, PBPI, is critical for cell division. **a** Growth profile of the CRISPRi *pbp1* knockdown strain. Data from a single growth curve experiment; mean and standard deviation plotted from three biological replicates. **b** Representative micrographs showing morphological and PG incorporation phenotypes of *pbp1* knockdown cells. Cells were grown in BHIS with or without xylose for 6–8 h. PG was labeled by incubation with HADA. Scale bar, 5 μm. Data representative of multiple independent experiments. **c** Moenomycin treatment of WT cultures. Moenomycin was added after two hours of growth as indicated, and cells were collected and fixed for imaging 2 h after treatment. Mean and range are plotted from two biological replicates. **d** Representative micrographs showing morphological and PG incorporation phenotypes of moenomycin-treated WT cells. PG was labeled by

incubation with HADA. Scale bar, 5 μm. Data representative of multiple independent experiments. **e** Representative phase-contrast and fluorescence micrographs showing PG incorporation and subcellular localization of mScarlet-PBPI in exponentially growing cells. PG was labeled by incubation with HADA, and mScarlet-*pbp1* was expressed using the native *pbp1* promoter from an ectopic locus. Scale bar, 5 μm. Similar patterns of localization were observed in multiple independent experiments. **f** Demograph showing fluorescence intensity across multiple cells representing subcellular localization of PBPI in exponentially growing cells. Cells are aligned at the mid-cell and sorted by length. Data are from 173 cells from one experiment and are representative of two independent experiments.

like *B. subtilis*^{23,24}, the SEDS and bPBP genes in the *C. difficile* *dcw* cluster play sporulation-specific roles (Fig. 2).

However, in contrast with *B. subtilis*, where SpoVE and SpoVD function exclusively during cortex synthesis, we have identified a novel role for SpoVE and SpoVD in mediating septal PG synthesis during asymmetric division in *C. difficile*. We posit that this additional function

for SpoVE and SpoVD reflects their ancestral role in cell division. Since the last common ancestor of the Firmicutes is thought to have been a spore-former²⁵, it is likely that this ancestor diversified the function of its *dcw*-encoded cell division PG synthases, FtsW and FtsI, to include both asymmetric division and cortex formation. According to this evolutionary scenario, *C. difficile* SpoVE and SpoVD represent an

intermediate form that has retained its involvement in asymmetric division and cortex synthesis, while *B. subtilis* SpoVE and SpoVD became exclusively specialized for cortex synthesis. This interpretation is supported by our data suggesting that the PG synthesizing function of *C. difficile* SpoVD and SpoVE during asymmetric division is regulated by the divisome components FtsL, FtsQ, and FtsB (Fig. 3), which are essential regulators of FtsW and FtsI in other organisms, including *B. subtilis*^{38–42}.

Notably, the specialization of *dcw*-encoded SEDS and bBPB enzymes in mediating PG transformations during spore formation in the Firmicutes required that these organisms develop or repurpose other enzymes to drive vegetative cell division. Sporulating members of the Bacilli encode an additional bBPB in the *dcw* cluster adjacent to *spoVD* (Fig. 1), which appears to encode a functional ortholog of FtsI and was likely a product of a gene duplication event. Similarly, the evolution of a functional ortholog of FtsW encoded outside the *dcw* cluster in the Bacilli was likely facilitated by a gene duplication or horizontal gene transfer event. In contrast, many members of the Clostridia appear to lack *ftsW* and *ftsI* orthologs (Fig. 1), so a non-SEDS-bBPB PG synthase, namely the aBPB, PBPI, likely evolved to mediate cell division independent of the canonical cell division machinery.

While it is unclear why the function of SpoVE and SpoVD during asymmetric division is not conserved in *B. subtilis* and likely other Bacilli, it appears that their roles in this critical process will likely be observed only in spore formers that lack functional FtsW and FtsI orthologs. This is consistent with our observation that, unlike *C. difficile* and most other Clostridia, the Bacilli and Negativicutes appear to encode functional orthologs of FtsW and FtsI (Fig. 1), which likely mediate both medial and asymmetric division. Interestingly, the *B. subtilis* aBPB PBPI is required for efficient septation during asymmetric division but not medial division⁵⁷, similar to how SpoVE-SpoVD are required for efficient asymmetric division in *C. difficile*. Given that the asymmetric division defects of *spoVD* and *spoVE* mutants in *C. difficile* are non-penetrant, it is likely that PBPI is also a major driver of septal PG synthesis during sporulation. These observations suggest that the formation of the division septum during asymmetric division may have requirements for both aBPB and SEDS-bBPB activities, which may contribute to the differences between medial and polar septa observed in *B. subtilis*⁵⁸.

While our results strongly suggest that the essential PG synthases in *C. difficile*, PBPI and RodA-PBP2, are functionally specialized to mediate cell division and elongation, respectively (Figs. 4, 5), it remains possible that these two distinct sets of PBPs participate in both processes. Indeed, PBPI likely contributes to general cell wall synthesis and maintenance independent of its role in septation, given that aPBPs in other bacteria can function autonomously from the divisome¹¹. This is supported by our observation of lower levels of HADA incorporation throughout the cell upon *pbp1* knockdown or moenomycin treatment (Fig. 5b, d). Furthermore, a recent study suggests that *C. difficile* PBPI transpeptidase activity is likely non-essential⁵⁹, in which case, PBP2 may provide the missing transpeptidase activity. Indeed, redundancy in transpeptidase activities during cell division has been described in *B. subtilis* and *S. aureus* and may be more widely conserved than currently appreciated^{8,60–62}.

Crucially, whether and how *C. difficile* PBPI activity is regulated during septal PG synthesis remains unclear. FtsL, FtsQ, and FtsB are dispensable during vegetative growth (Fig. 3), and *C. difficile* lacks homologs of FtsA and FtsN, which regulate divisome assembly and PG synthesis activity in many bacteria¹. Thus, factors that substitute for the function of these widely conserved divisome proteins remain to be discovered. Interestingly, a cluster of three genes encoding mid cell-localizing proteins (MldABC) unique to *C. difficile* and closely related organisms appear to be important for cell division⁶³. Since one of these proteins (MldA) contains a PG-binding SPOR domain which is commonly found in components of the divisome in other bacteria and was

recently implicated in regulating aBPB activity in *E. coli*⁶⁴, Mld proteins may be involved in regulating septal PG synthesis by PBPI. However, further study is required to define the components of the distinct divisome encoded by *C. difficile*.

Altogether, our findings provide novel insight into the evolution of PG-synthesizing enzymes in the Firmicutes and highlight the diversity of PG synthesis mechanisms employed by bacteria. These observations may explain some of the disparities in cell division mechanisms reported for model Firmicutes organisms such as *B. subtilis* and *S. aureus* compared to non-Firmicutes models such as *E. coli*, including differences in FtsW-FtsI enzyme dynamics and aBPB function in relation to the divisome¹⁹. Moreover, by revealing unique characteristics of *C. difficile*'s cell division machinery during sporulation and vegetative growth, these analyses may inform the development of more specific therapeutics against this important pathogen.

Methods

Gene synteny, homology searches, and phylogenetic analyses

Genomic loci containing *dcw* clusters shown in Fig. 1 were manually determined by searching for *dcw* genes (*mraZ*, *ftsW/spoVE*, *ftsZ*) and extracted from genomes in the Genbank database (accession numbers and coordinates are listed in Supplementary Data 1). Gene neighborhoods were visualized using Clinker⁶⁵ on the GAGECAT web server (<https://cagecat.bioinformatics.nl/tools/clinker>)⁶⁶.

For all other analyses presented in Supplementary Figs. 1 and 2 and Supplementary Data 3, we assembled a local databank of Firmicutes by selecting one proteome per genus as performed by ref. 67. Proteome selection was realized considering genome characteristics such as assembly level and category. The assembled databank contains 494 genomes listed in Supplementary Data 2. In order to build a reference phylogeny, exhaustive HMM-based homology searches (with the option `--cut_ga`) were carried out by using HMM profiles of bacterial ribosomal proteins from the Pfam 29.0 database as queries on the Firmicutes databank using the HMMER-3.1b2 package (hmmer.org)⁶⁸. The conserved ribosomal proteins were aligned with MAFFT-v7.407 with the auto option and trimmed using BMGE-1.1⁶⁹. The resulting trimmed alignments were concatenated into a supermatrix (497 taxa and 3776 amino acid positions). A maximum likelihood tree was generated using IQTREE-1.6.3⁷⁰ under the LG+I+G4 model with 1000 ultrafast bootstrap replicates.

Homology searches were performed using HMMSEARCH from the HMMER-3.1b2 package to screen all the proteomes in the Firmicutes databank for the presence of SpoOA, SpoIIE, SEDS glycosyltransferases, and bBPB homologs. We used the Pfam database to retrieve Pfam domains PF08769, PF07228, PF01098, and PF00905 for SpoOA, SpoIIE, SEDS glycosyltransferases, and bBPB respectively⁷¹. All hits were then manually curated using phylogeny and domain organization to discard false positives. For SEDS and bBPB sets of hits, the kept sequences were aligned with MAFFT v7.481 (`--auto`)⁷², trimmed with trimAl 1.2rev59⁷³ and single gene trees were built using IQ-TREE v2.0.7⁷⁴ with best-fit model chosen according to BIC criterium.

We next used MacSyFinder2⁷⁵ to locate the hits in the genomes. We assessed the genes as located in the *dcw* cluster when at least four out of the genes *ftsW/spoVE*, *ftsI/spoVD*, *ftsA*, *mraW*, *mraY*, *ftsZ*, *mraZ*, and *murCDEF* cooccurred in the genome separated by no more than five other genes. The *rodA-mrdA* pair located out of the *dcw* cluster was assessed when they were found separated by no more than five other genes with the absence of *mraW* and *mraY* in their close synteny. Finally, we identified the pair *ftsW-pycA* when the two genes cooccurred in the genome, separated by no more than 3 other genes. The presence or absence of the studied proteins and their synteny in the genomes were mapped onto the trees using ITOI⁷⁶.

The Jaccard similarity coefficients reported in Supplementary Data 3 were calculated using R and RStudio Version 1.4.1717 using the dataset from Supplementary Data 2. The Jaccard similarity coefficient

for each pairwise comparison was calculated by dividing the number of shared organisms by the total number of organisms in the two sets being compared.

***C. difficile* strain construction and growth conditions**

All *C. difficile* strains used in the study are derivatives of 630 Δ erm. Mutant strains were constructed in a 630 Δ erm Δ pyrE strain using pyrE-based allele-coupled exchange as previously described⁷⁷. All strains used in the study are reported in Supplementary Data 4. *C. difficile* strains were grown from frozen glycerol stocks on brain heart infusion-supplemented (BHIS) agar plates with taurocholate (TA, 0.1% w/v). *C. difficile* strains harboring pIA33- or pRPF185-based plasmids were grown on media supplemented with thiamphenicol (10 μ g/mL in liquid cultures and 5 μ g/mL in agar plates). Cultures were grown at 37 °C under anaerobic conditions using a gas mixture containing 85% N₂, 5% CO₂, and 10% H₂.

***E. coli* strain constructions**

Supplementary Data 5 lists all plasmids used in the study, with links to plasmid maps containing all primer sequences used for cloning. Plasmids were cloned via Gibson assembly, and cloned plasmids were transformed into *E. coli* (DH5 α or XL1-Blue strains). All plasmids were confirmed by sequencing the inserted region. Confirmed plasmids were transformed into the *E. coli* HB101 strain for conjugation with *C. difficile*. All *E. coli* HB101 strains used for conjugation are also listed in Supplementary Data 5.

Plate-based sporulation assays

For assays requiring sporulating cells, cultures were grown to early stationary phase, back-diluted 1:50 into BHIS, and grown until they reached an OD₆₀₀ between 0.35 and 0.75. 120 μ L of this culture was spread onto 70:30 (70% SMC media and 30% BHIS media) or SMC agar plates as indicated (40 ml media per plate). Sporulating cells were scraped from the plate and collected into phosphate-buffered saline (PBS), and sporulation levels were visualized by phase-contrast microscopy as previously described⁷⁸.

Heat resistance assay

Heat-resistant spore formation was measured 18–22 h after sporulation induction on 70:30 agar plates by resuspending a sample of sporulating cells in PBS, dividing the sample into two, heat-treating one of the samples at 60 °C for 30 min, and comparing the colony forming units (CFUs) in the untreated sample to the heat-treated sample⁷⁹. Heat-resistance efficiencies represent the average ratio of heat-resistant CFUs to total CFUs for a given strain relative to the average ratio for the wild-type strain.

Western blot analysis

Samples were collected 17 h after sporulation induction on 70:30 agar plates and processed for immunoblotting. Sample processing involved multiple freeze-thaws in PBS followed by the addition of EBB buffer (9 M urea, 2 M thiourea, 4% SDS, 2 mM β -mercaptoethanol), boiling, pelleting, resuspension, and boiling again prior to loading on a gel. σ^F , σ^E , and Spo0A were resolved using 15% SDS–polyacrylamide gel electrophoresis (SDS–PAGE) gels, whereas SpoVD and SpoIVA were resolved using 12% SDS–PAGE gels. Proteins were transferred to polyvinylidene difluoride membranes, which were subsequently probed with rabbit (anti-SigF³⁶, anti-SigE³⁶, and anti-SpoVD; all at 1:1000 dilution) and mouse (anti-Spo0A³⁶ (1:1000 dilution) and anti-SpoIVA³⁶ (1:3000 dilution)) polyclonal primary antibodies, and anti-rabbit IR800 and anti-mouse IR680 secondary antibodies (LI-COR Biosciences, 1:20,000 dilution). Blots were imaged using a LiCor Odyssey CLx imaging system. The results shown are representative of multiple experiments.

RT-qPCR analysis

RNA was harvested from sporulating cells 10–11 h after sporulating induction on 70:30 agar plates. Total RNA was processed according to published protocols³⁶. Briefly, RNA was harvested using FastRNA Pro Blue Kit; DNA was removed by multiple DNase I treatments, and mRNA was enriched using a MICROBExpress Bacterial mRNA Enrichment Kit for mRNA enrichment. Transcript levels were determined from cDNA templates prepared from a single experiment with three biological replicates per sample. Gene-specific primer pairs are provided in Supplementary Data 6. RT–qPCR was performed, using iTaq Universal SYBR Green supermix (BioRad), 50 nM of gene-specific primers, and an Mx3005P qPCR system (Stratagene) in a total volume of 25 μ L⁸⁰. The following cycling conditions were used: 95 °C for 2 min, followed by 40 cycles of 95 °C for 15 s and 60 °C for 1 min. Statistical tests were performed using GraphPad Prism (GraphPad Software, San Diego, CA, USA).

Bacterial two-hybrid analyses

Bacterial adenylate cyclase two-hybrid (BACTH) assays were performed using *E. coli* BTH101 cells as previously described⁸¹. BTH101 cells were freshly transformed with 100 ng of each BACTH assay plasmid and plated on fresh LB agar plates supplemented with 50 μ g/ml kanamycin, 100 μ g/ml Ampicillin, and 0.5 mM isopropyl β -D-thiogalactopyranoside (IPTG). Plates were incubated for 64–68 h at 30 °C, and β -galactosidase activity was quantified in Miller units as previously detailed⁸². The β -galactosidase activity of cells transformed with the empty pUT18C and pKT25 vectors was used as a negative control for normalization.

Growth curve assays

For each replicate of the growth assay shown in Fig. 5c, a mid-log culture was normalized to a starting OD₆₀₀ ~0.05. After two hours of growth, the culture was aliquoted into three separate tubes and supplemented with moenomycin as indicated. The OD₆₀₀ value of each culture was measured every hour using a portable colorimeter (Biochrom WPA CO7500). For all other growth assays, stationary phase cultures were back-diluted 1:50 in BHIS and grown to mid-log phase (OD₆₀₀ 0.5). Log-phase cultures were normalized to a starting OD₆₀₀ ~0.01 and distributed into wells (150 μ L per well) of a 96-well plate. The plate was incubated in an Epoch microplate spectrophotometer (Agilent BioTek) at 37 °C with linear shaking for 2 min prior to each time point. The OD₆₀₀ value for each well was recorded every 15 min. For growth assays involving strains with pIA33- or pRPF185-based plasmids, media was supplemented with 10 μ g/mL thiamphenicol and either xylose or anhydrotetracycline as indicated. For assays involving moenomycin treatment, cultures were supplemented with different concentrations of moenomycin as indicated.

Nucleoid, membrane, and cell wall labeling

Fluorescence microscopy was performed on sporulating cells using Hoechst 33342 (Molecular Probes; 15 μ g ml⁻¹) and FM4-64 (Invitrogen; 1 μ g ml⁻¹) to stain nucleoid and membrane, respectively. For cell wall labeling, HADA (Tocris Bioscience) was added to exponentially growing cell culture to a final concentration of 100–200 μ M and incubated for ~2 min before cell fixation.

Cell fixation

Cells were fixed by taking an 800 μ L of culture in BHIS media and adding 200 μ L of a 5 \times fixation solution containing paraformaldehyde and NaPO₄ buffer⁸³. Samples were mixed and incubated in the dark for 30 min at room temperature, followed by 30 min on ice. Fixed cells were washed three times in PBS and resuspended in an appropriate volume of PBS depending on cellular density. Cells were imaged within 72 h after fixation.

Microscope hardware

All samples for a given experiment were imaged from a single agar pad (1.5% low-melting point agarose in PBS). Phase-contrast micrographs shown in Supplementary Fig. 3 were acquired using a Zeiss Axioskop upright microscope with a 100× Plan-NEOFLUAR oil-immersion phase-contrast objective and a Hamamatsu C4742-95 Orca 100 CCD Camera. All other phase-contrast and fluorescence micrographs were obtained using a Leica DMi8 inverted microscope equipped with a 63× 1.4 NA Plan Apochromat oil-immersion phase-contrast objective, a high precision motorized stage (Pecon), and an incubator (Pecon) set at 37 °C. Excitation light was generated by a Lumencor Spectra-X multi-LED light source with integrated excitation filters. An XLED-QP quadruple-band dichroic beam-splitter (Leica) was used (transmission: 415, 470, 570, and 660 nm) with an external filter wheel for all fluorescent channels. FM4-64 was excited at 550/38 nm, and emitted light was filtered using a 705/72-nm emission filter (Leica); HADA and Hoechst were excited at 395/40, and emitted light was filtered using a 440/40-nm emission filter (Leica); mScarlet was excited at 550/38 nm, and emitted light was filtered using a 590/50-nm emission filter (Leica). Emitted and transmitted light was detected using a Leica DFC 9000 GTC sCMOS camera. 1 to 2 μm z-stacks were taken when needed with 0.21 μm z-slices.

Microscopy image analyses

Images were acquired and exported using the LASX software. To avoid bleed-through of fluorescent signal into neighboring cells, a background subtraction method (Leica Instant Computational Clearing) was applied to the fluorescence images used for fluorescent reporter analyses shown in Fig. 2e, f and Supplementary Fig. 5. All other images were exported without further processing. After export, images were processed using Fiji⁸⁴ to remove out-of-focus regions via cropping. The best-focused Z-planes for all channels were manually selected to correct for any chromatic aberration. Image scaling was adjusted to improve brightness and contrast for display and was applied equally to all images shown in a single panel. For cell segmentation and quantification of length and fluorescent intensities, the MATLAB-based image analysis pipeline SuperSegger⁸⁵ was used with the default 60× settings. Data used for fluorescent reporter analyses shown in Fig. 2e, f and Supplementary Fig. 5 were filtered to remove spore particles by length and cells at image border by XY position. Visualization of quantified data and any associated statistical tests were performed using Prism 10 (GraphPad Software, San Diego, CA, USA).

Segmentation of cells and fluorescent intensity analyses used to generate data shown in Fig. 5f to analyze mScarlet-PBP1 localization were conducted using the MicrobeJ plugin⁸⁶ in ImageJ. Analyses of SpoVD-mScarlet localization and HADA incorporation in asymmetrically dividing cells shown in Supplementary Fig. 5 were conducted in ImageJ. Individual cells undergoing asymmetric division were isolated by manually identifying cells with a polar septum in the HADA channel. A 5-pixel wide pole-to-pole vector was drawn to gather fluorescent intensities across the cell. For each channel, the fluorescent intensity was normalized to the minimum and maximum values for each cell and plotted against the normalized cell length.

Transmission electron microscopy

Sporulating cells were collected ~22 h after sporulation induction on 70:30 or SMC agar plates. Cells were fixed and processed for electron microscopy by the University of Vermont Microscopy Center⁸⁷. Briefly, sporulating cultures were fixed in 2% glutaraldehyde, 2% paraformaldehyde in 0.1 M sodium cacodylate buffer, washed in 0.1 M cacodylate buffer, embedded in agarose, cross-linked with Karnovsky's buffer (1% paraformaldehyde, 2.5% glutaraldehyde in 0.1 M cacodylate buffer), washed in 0.1 M cacodylate buffer, and minced into 1 mm³ pieces. Samples were dehydrated through graded ethanols (35%, 50%, 70%, 85%, and 95%) and cleared twice in 100% propylene oxide. Samples were infiltrated with Spurr's epoxy resin (100%

polypropylene oxide) with increasing ratios, and embedded in Spurr's resin at 70 °C prior to sectioning. Semi-thin sections (1 μm) were cut on a Reichert Ultracut Microtome, stained with methylene blue-azure II, and evaluated for areas of interest. Ultra-thin sections (60–80 nm) were cut with a diamond knife, retrieved onto 200 mesh thin bar nickel grids, contrasted with uranyl acetate (2% in 50% ethanol) and Reynold's lead citrate. All TEM images were captured on a JEOL 1400 Transmission Electron Microscope (Jeol USA, Inc., Peabody, MA) with an AMT XR611 high-resolution 11-megapixel mid-mount CCD camera.

Reporting summary

Further information on research design is available in the Nature Portfolio Reporting Summary linked to this article.

Data availability

Data used to generate graphs, exact *P* values from statistical analyses, and uncropped scans of blots can be accessed in the Source Data file. All other data supporting the findings of this study are available within the article, Supplementary Data and Supplementary Information file. Any associated unprocessed data are available upon request. The Genbank and Pfam 29.0 databases were used in this study. Source data are provided with this paper.

References

- Egan, A. J. F., Errington, J. & Vollmer, W. Regulation of peptidoglycan synthesis and remodelling. *Nat. Rev. Microbiol.* **18**, 446–460 (2020).
- Meeske, A. J. et al. SEDS proteins are a widespread family of bacterial cell wall polymerases. *Nature* **537**, 634–638 (2016).
- Cho, H. et al. Bacterial cell wall biogenesis is mediated by SEDS and PBP polymerase families functioning semi-autonomously. *Nat. Microbiol.* **1**, 1–8 (2016).
- Emami, K. et al. RodA as the missing glycosyltransferase in *Bacillus subtilis* and antibiotic discovery for the peptidoglycan polymerase pathway. *Nat. Microbiol.* **2**, 1–9 (2017).
- Taguchi, A. et al. FtsW is a peptidoglycan polymerase that is functional only in complex with its cognate penicillin-binding protein. *Nat. Microbiol.* **4**, 587–594 (2019).
- Sjodt, M. et al. Structural coordination of polymerization and crosslinking by a SEDS–bPBP peptidoglycan synthase complex. *Nat. Microbiol.* **5**, 813–820 (2020).
- Leclercq, S. et al. Interplay between penicillin-binding proteins and SEDS proteins promotes bacterial cell wall synthesis. *Sci. Rep.* **7**, 43306 (2017).
- Reichmann, N. T. et al. SEDS–bPBP pairs direct lateral and septal peptidoglycan synthesis in *Staphylococcus aureus*. *Nat. Microbiol.* **4**, 1368–1377 (2019).
- Straume, D., Piechowiak, K. W., Kjos, M. & Håvarstein, L. S. Class A PBPs: It is time to rethink traditional paradigms. *Mol. Microbiol.* **116**, 41–52 (2021).
- Dion, M. F. et al. *Bacillus subtilis* cell diameter is determined by the opposing actions of two distinct cell wall synthetic systems. *Nat. Microbiol.* **4**, 1294–1305 (2019).
- Vigouroux, A. et al. Class-A penicillin binding proteins do not contribute to cell shape but repair cell-wall defects. *eLife* **9**, e51998 (2020).
- Straume, D. et al. Class A PBPs have a distinct and unique role in the construction of the pneumococcal cell wall. *Proc. Natl. Acad. Sci.* **117**, 6129–6138 (2020).
- Atwal, S. et al. Discovery of a diverse set of bacteria that build their cell walls without the canonical peptidoglycan polymerase aPBP. *mBio* **12**, e01342–21 (2021).
- Joyce, G. et al. Cell division site placement and asymmetric growth in mycobacteria. *PLOS One* **7**, e44582 (2012).

15. Kieser, K. J. et al. Phosphorylation of the peptidoglycan synthase PonA1 governs the rate of polar elongation in mycobacteria. *PLoS Pathog.* **11**, e1005010 (2015).
16. Sher, J. W., Lim, H. C. & Bernhardt, T. G. Polar growth in *Corynebacterium glutamicum* has a flexible cell wall synthase requirement. *mBio* e0068221 (2021).
17. Williams, M. A. et al. Unipolar peptidoglycan synthesis in the Rhizobiales requires an essential class A penicillin-binding protein. *mBio* **12**, e02346–21 (2021).
18. Megrian, D., Taib, N., Jaffe, A. L., Banfield, J. F. & Gribaldo, S. Ancient origin and constrained evolution of the division and cell wall gene cluster in Bacteria. *Nat. Microbiol.* **7**, 2114–2127 (2022).
19. Piggot, P. J. & Coote, J. G. Genetic aspects of bacterial endospore formation. *Microbiol. Mol. Biol. Rev.* **40**, 908–962 (1976).
20. Ikeda, M. et al. Structural similarity among *Escherichia coli* FtsW and RodA proteins and *Bacillus subtilis* SpoVE protein, which function in cell division, cell elongation, and spore formation, respectively. *J. Bacteriol.* **171**, 6375–6378 (1989).
21. Henriques, A. O., de Lencastre, H. & Piggot, P. J. A *Bacillus subtilis* morphogene cluster that includes *spoVE* is homologous to the *mra* region of *Escherichia coli*. *Biochimie* **74**, 735–748 (1992).
22. Yanouri, A., Daniel, R. A., Errington, J. & Buchanan, C. E. Cloning and sequencing of the cell division gene *pbpB*, which encodes Penicillin-Binding Protein 2B in *Bacillus subtilis*. *J. Bacteriol.* **175**, 7604–7616 (1993).
23. Daniel, R. A., Drake, S., Buchanan, C. E., Scholle, R. & Errington, J. The *Bacillus subtilis* *spoVD* gene encodes a mother-cell-specific penicillin-binding protein required for spore morphogenesis. *J. Mol. Biol.* **235**, 209–220 (1994).
24. Fay, A., Meyer, P. & Dworkin, J. Interactions between late-acting proteins required for peptidoglycan synthesis during sporulation. *J. Mol. Biol.* **399**, 547–561 (2010).
25. Garcia, P. S. et al. A comprehensive evolutionary scenario of cell division and associated processes in the Firmicutes. *Mol. Biol. Evol.* **38**, 2396–2412 (2021).
26. Galperin, M. Y., Yutin, N., Wolf, Y. I., Vera Alvarez, R. & Koonin, E. V. Conservation and evolution of the sporulation gene set in diverse members of the Firmicutes. *J. Bacteriol.* **204**, e00079–22 (2022).
27. Ferrari, F. A. et al. Characterization of the *spoOA* locus and its deduced product. *Proc. Natl. Acad. Sci. USA* **82**, 2647–2651 (1985).
28. Margolis, P., Driks, A. & Losick, R. Establishment of cell type by compartmentalized activation of a transcription factor. *Science* **254**, 562–565 (1991).
29. Perez, A. J. et al. Movement dynamics of divisome proteins and PBP2x:FtsW in cells of *Streptococcus pneumoniae*. *Proc. Natl. Acad. Sci.* **116**, 3211–3220 (2019).
30. Rismondo, J., Halbedel, S. & Gründling, A. Cell shape and antibiotic resistance are maintained by the activity of multiple FtsW and RodA enzymes in *Listeria monocytogenes*. *mBio* **10**, e01448–19 (2019).
31. Dembek, M. et al. High-throughput analysis of gene essentiality and sporulation in *Clostridium difficile*. *mBio* **6**, e02383 (2015).
32. Srikhanta, Y. N. et al. Cephamycins inhibit pathogen sporulation and effectively treat recurrent *Clostridioides difficile* infection. *Nat. Microbiol.* **4**, 2237–2245 (2019).
33. Alabdali, Y. A. J., Oatley, P., Kirk, J. A. & Fagan, R. P. A cortex-specific penicillin-binding protein contributes to heat resistance in *Clostridioides difficile* spores. *Anaerobe* **70**, 102379 (2021).
34. Pogliano, J. et al. A vital stain for studying membrane dynamics in bacteria: a novel mechanism controlling septation during *Bacillus subtilis* sporulation. *Mol. Microbiol.* **31**, 1149–1159 (1999).
35. Nonejuie, P., Burkart, M., Pogliano, K. & Pogliano, J. Bacterial cytological profiling rapidly identifies the cellular pathways targeted by antibacterial molecules. *Proc. Natl. Acad. Sci.* **110**, 16169–16174 (2013).
36. Firmlaid, K. A. et al. Global analysis of the sporulation pathway of *Clostridium difficile*. *PLoS Genet.* **9**, e1003660 (2013).
37. Saujet, L. et al. Genome-wide analysis of cell type-specific gene transcription during spore formation in *Clostridium difficile*. *PLOS Genet.* **9**, e1003756 (2013).
38. Levin, P. A. & Losick, R. Characterization of a cell division gene from *Bacillus subtilis* that is required for vegetative and sporulation septum formation. *J. Bacteriol.* **176**, 1451–1459 (1994).
39. Daniel, R. A., Harry, E. J., Katis, V. L., Wake, R. G. & Errington, J. Characterization of the essential cell division gene *ftsL* (*yIIID*) of *Bacillus subtilis* and its role in the assembly of the division apparatus. *Mol. Microbiol.* **29**, 593–604 (1998).
40. Katis, V. L. & Wake, R. G. Membrane-bound division proteins DivIB and DivIC of *Bacillus subtilis* function solely through their external domains in both vegetative and sporulation division. *J. Bacteriol.* **181**, 2710–2718 (1999).
41. Tsang, M. J. & Bernhardt, T. G. A role for the FtsQLB complex in cytokinetic ring activation revealed by an *ftsL* allele that accelerates division. *Mol. Microbiol.* **95**, 925–944 (2015).
42. Marmont, L. S. & Bernhardt, T. G. A conserved subcomplex within the bacterial cytokinetic ring activates cell wall synthesis by the FtsW-FtsI synthase. *Proc. Natl. Acad. Sci.* **117**, 23879–23885 (2020).
43. Beall, B. & Lutkenhaus, J. Nucleotide sequence and insertional inactivation of a *Bacillus subtilis* gene that affects cell division, sporulation, and temperature sensitivity. *J. Bacteriol.* **171**, 6821–6834 (1989).
44. Le Gouëllec, A. et al. Roles of Pneumococcal DivIB in cell division. *J. Bacteriol.* **190**, 4501–4511 (2008).
45. Masson, S. et al. Central domain of DivIB caps the C-terminal regions of the FtsL/DivIC coiled-coil rod. *J. Biol. Chem.* **284**, 27687–27700 (2009).
46. Thompson, L. S., Beech, P. L., Real, G., Henriques, A. O. & Harry, E. J. Requirement for the cell division protein DivIB in polar cell division and engulfment during sporulation in *Bacillus subtilis*. *J. Bacteriol.* **188**, 7677–7685 (2006).
47. Di Lallo, G., Fagioli, M., Barionovi, D., Ghelardini, P. & Paolozzi, L. Y. Use of a two-hybrid assay to study the assembly of a complex multicomponent protein machinery: bacterial septosome differentiation. *Microbiology* **149**, 3353–3359 (2003).
48. Karimova, G., Dautin, N. & Ladant, D. Interaction network among *Escherichia coli* membrane proteins involved in cell division as revealed by bacterial two-hybrid analysis. *J. Bacteriol.* **187**, 2233–2243 (2005).
49. Maggi, S. et al. Division protein interaction web: identification of a phylogenetically conserved common interactome between *Streptococcus pneumoniae* and *Escherichia coli*. *Microbiology* **154**, 3042–3052 (2008).
50. Robichon, C., King, G. F., Goehring, N. W. & Beckwith, J. Artificial septal targeting of *Bacillus subtilis* cell division proteins in *Escherichia coli*: an interspecies approach to the study of protein-protein interactions in multiprotein complexes. *J. Bacteriol.* **190**, 6048–6059 (2008).
51. Müh, U., Pannullo, A. G., Weiss, D. S. & Ellermeier, C. D. A Xylose-inducible expression system and a CRISPR interference plasmid for targeted knockdown of gene expression in *Clostridioides difficile*. *J. Bacteriol.* **201**, e00711–e00718 (2019).
52. Matsuzawa, H., Hayakawa, K., Sato, T. & Imahori, K. Characterization and genetic analysis of a mutant of *Escherichia coli* K-12 with rounded morphology. *J. Bacteriol.* **115**, 436–442 (1973).
53. Spratt, B. G. Distinct penicillin binding proteins involved in the division, elongation, and shape of *Escherichia coli* K12. *Proc. Natl. Acad. Sci.* **72**, 2999–3003 (1975).
54. Murray, T., Popham, D. L. & Setlow, P. Identification and characterization of *pbpA* encoding *Bacillus subtilis* Penicillin-Binding Protein 2A. *J. Bacteriol.* **179**, 3021–3029 (1997).

55. Henriques, A. O., Glaser, P., Piggot, P. J. & Moran, C. P. Jr Control of cell shape and elongation by the *rodA* gene in *Bacillus subtilis*. *Mol. Microbiol.* **28**, 235–247 (1998).
56. Cheng, T. J. R. et al. Domain requirement of moenomycin binding to bifunctional transglycosylases and development of high-throughput discovery of antibiotics. *Proc. Natl. Acad. Sci.* **105**, 431–436 (2008).
57. Scheffers, D. J. & Errington, J. PBP1 is a component of the *Bacillus subtilis* cell division machinery. *J. Bacteriol.* **186**, 5153–5156 (2004).
58. Khanna, K., Lopez-Garrido, J., Sugie, J., Pogliano, K. & Villa, E. Asymmetric localization of the cell division machinery during *Bacillus subtilis* sporulation. *eLife* **10**, e62204 (2021).
59. Sacco, M. D. et al. A unique class of Zn²⁺-binding serine-based PBPs underlies cephalosporin resistance and sporogenesis in *Clostridioides difficile*. *Nat. Commun.* **13**, 4370 (2022).
60. Pinho, M. G., Filipe, S. R., de Lencastre, H. & Tomasz, A. Complementation of the essential peptidoglycan transpeptidase function of Penicillin-Binding Protein 2 (PBP2) by the drug resistance protein PBP2A in *Staphylococcus aureus*. *J. Bacteriol.* **183**, 6525–6531 (2001).
61. Sassine, J. et al. Functional redundancy of division specific penicillin-binding proteins in *Bacillus subtilis*. *Mol. Microbiol.* **106**, 304–318 (2017).
62. Wacnik, K. et al. Penicillin-Binding Protein 1 (PBP1) of *Staphylococcus aureus* has multiple essential functions in cell division. *mBio* **13**, e00669–22 (2022).
63. Ransom, E. M., Williams, K. B., Weiss, D. S. & Ellermeier, C. D. Identification and characterization of a gene cluster required for proper rod shape, cell division, and pathogenesis in *Clostridium difficile*. *J. Bacteriol.* **196**, 2290–2300 (2014).
64. Pazos, M. et al. SPOR proteins are required for functionality of class A penicillin-binding proteins in *Escherichia coli*. *mBio* **11**, e02796–20 (2020).
65. Gilchrist, C. L. M. & Chooi, Y. H. clinker & clustermap.js: automatic generation of gene cluster comparison figures. *Bioinformatics* **37**, 2473–2475 (2021).
66. van den Belt, M. et al. CAGECAT: the CompArative GENE Cluster Analysis Toolbox for rapid search and visualisation of homologous gene clusters. *BMC Bioinform.* **24**, 181 (2023).
67. Luhur, J. et al. A dynamic, ring-forming MucB/RseB-like protein influences spore shape in *Bacillus subtilis*. *PLOS Genet.* **16**, e1009246 (2020).
68. Johnson, L. S., Eddy, S. R. & Portugaly, E. Hidden Markov model speed heuristic and iterative HMM search procedure. *BMC Bioinform.* **11**, 431 (2010).
69. Criscuolo, A. & Grubaldo, S. BMGE (Block Mapping and Gathering with Entropy): a new software for selection of phylogenetic informative regions from multiple sequence alignments. *BMC Evol. Biol.* **10**, 210 (2010).
70. Nguyen, L. T., Schmidt, H. A., von Haeseler, A. & Minh, B. Q. IQ-TREE: a fast and effective stochastic algorithm for estimating maximum-likelihood phylogenies. *Mol. Biol. Evol.* **32**, 268–274 (2015).
71. Finn, R. D. et al. The Pfam protein families database: towards a more sustainable future. *Nucleic Acids Res.* **44**, D279–D285 (2016).
72. Katoh, K. & Standley, D. M. MAFFT multiple sequence alignment software version 7: improvements in performance and usability. *Mol. Biol. Evol.* **30**, 772–780 (2013).
73. Capella-Gutiérrez, S., Silla-Martínez, J. M. & Gabaldón, T. trimAl: a tool for automated alignment trimming in large-scale phylogenetic analyses. *Bioinformatics* **25**, 1972–1973 (2009).
74. Minh, B. Q. et al. IQ-TREE 2: new models and efficient methods for phylogenetic inference in the genomic era. *Mol. Biol. Evol.* **37**, 1530–1534 (2020).
75. Néron, B. et al. MacSyFinder v2: Improved modelling and search engine to identify molecular systems in genomes. *Peer Commun. J.* **3**, e28 (2023).
76. Letunic, I. & Bork, P. Interactive Tree Of Life (iTOL) v5: an online tool for phylogenetic tree display and annotation. *Nucleic Acids Res.* **49**, W293–W296 (2021).
77. Ng, Y. K. et al. Expanding the repertoire of gene tools for precise manipulation of the *Clostridium difficile* genome: allelic exchange using *pyrE* Alleles. *PLOS One* **8**, e56051 (2013).
78. Pishdadian, K., Fimlaid, K. A. & Shen, A. SpoIIID-mediated regulation of σ^E function during *Clostridium difficile* sporulation. *Mol. Microbiol.* **95**, 189–208 (2015).
79. Fimlaid, K. A. et al. Identification of a Novel Lipoprotein regulator of *Clostridium difficile* spore germination. *PLOS Pathog.* **11**, e1005239 (2015).
80. Oliveira, P. H. et al. Epigenomic characterization of *Clostridioides difficile* finds a conserved DNA methyltransferase that mediates sporulation and pathogenesis. *Nat. Microbiol.* **5**, 166–180 (2020).
81. Karimova, G., Pidoux, J., Ullmann, A. & Ladant, D. A bacterial two-hybrid system based on a reconstituted signal transduction pathway. *Proc. Natl. Acad. Sci.* **95**, 5752–5756 (1998).
82. Dahlstrom, K. M., Giglio, K. M., Collins, A. J., Sondermann, H. & O’Toole, G. A. Contribution of physical interactions to signaling specificity between a diguanylate cyclase and its effector. *mBio* **6**, e01978–15 (2015).
83. Ransom, E. M., Weiss, D. S. & Ellermeier, C. D. Use of mCherryOpt Fluorescent Protein in *Clostridium difficile*. *Methods Mol. Biol.* **1476**, 53–67 (2016).
84. Schindelin, J. et al. Fiji: an open-source platform for biological-image analysis. *Nat. Methods* **9**, 676–682 (2012).
85. Stylianidou, S., Brennan, C., Nissen, S. B., Kuwada, N. J. & Wiggins, P. A. SuperSegger: robust image segmentation, analysis and lineage tracking of bacterial cells. *Mol. Microbiol.* **102**, 690–700 (2016).
86. Ducret, A., Quardokus, E. M. & Brun, Y. V. MicrobeJ, a tool for high throughput bacterial cell detection and quantitative analysis. *Nat. Microbiol.* **1**, 1–7 (2016).
87. Putnam, E. E., Nock, A. M., Lawley, T. D. & Shen, A. SpoIVA and Sipl are *Clostridium difficile* spore morphogenetic proteins. *J. Bacteriol.* **195**, 1214–1225 (2013).

Acknowledgements

We acknowledge the University of Vermont Microscopy Imaging Core for processing the samples and acquiring the images for all Transmission Electron Microscopy analyses. We thank Craig D. Ellermeier, David S. Weiss, and Ute Müh for their input on the project and for sharing protocols and plasmids used in the study. We are grateful to members of the Shen lab for helpful discussions and feedback on the manuscript. The National Institute of Allergy and Infectious Diseases grant R01 AI122232 (to A.S.), and Burroughs Wellcome Fund for Investigators in Pathogenesis Award (to A.S.) provided funding for this work.

Author contributions

S.S. and A.S. conceived the study. S.S. performed and analyzed experiments. S.S. and N.T. conducted bioinformatic analyses. A.S. supervised the study. S.S. and A.S. wrote the manuscript with input from N.T. and S.G. All authors reviewed and approved the manuscript.

Competing interests

The authors declare no competing interests.

Additional information

Supplementary information The online version contains supplementary material available at <https://doi.org/10.1038/s41467-023-43595-3>.

Correspondence and requests for materials should be addressed to Aimee Shen.

Peer review information *Nature Communications* thanks Imrich Barák and the other, anonymous, reviewers for their contribution to the peer review of this work. A peer review file is available.

Reprints and permissions information is available at <http://www.nature.com/reprints>

Publisher's note Springer Nature remains neutral with regard to jurisdictional claims in published maps and institutional affiliations.

Open Access This article is licensed under a Creative Commons Attribution 4.0 International License, which permits use, sharing, adaptation, distribution and reproduction in any medium or format, as long as you give appropriate credit to the original author(s) and the source, provide a link to the Creative Commons license, and indicate if changes were made. The images or other third party material in this article are included in the article's Creative Commons license, unless indicated otherwise in a credit line to the material. If material is not included in the article's Creative Commons license and your intended use is not permitted by statutory regulation or exceeds the permitted use, you will need to obtain permission directly from the copyright holder. To view a copy of this license, visit <http://creativecommons.org/licenses/by/4.0/>.

© The Author(s) 2023